CHALMERS
UNIVERSITY OF TECHNOLOGY

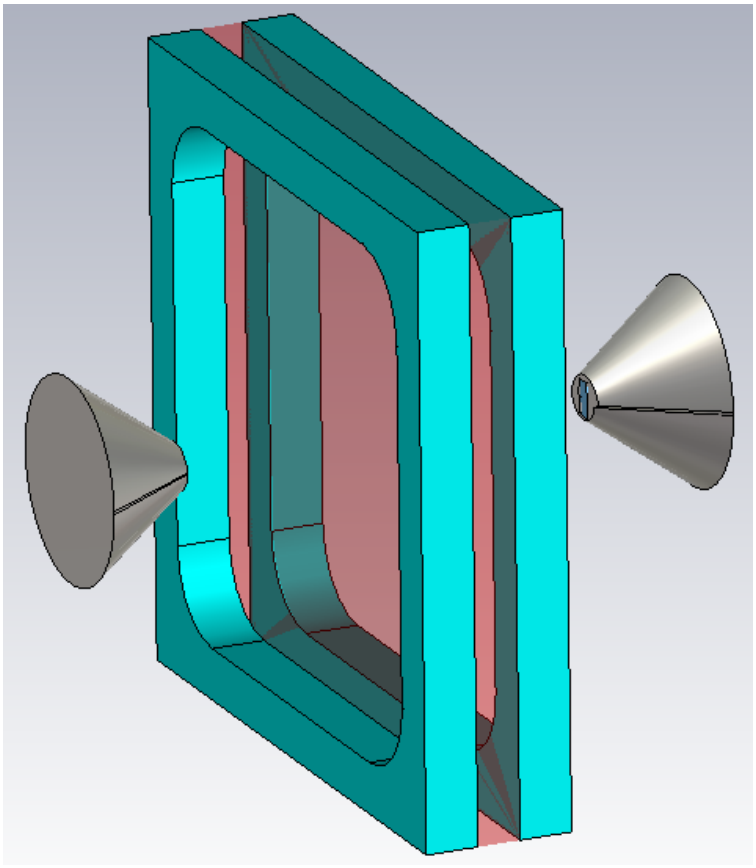

THz Imaging of Roll Compaction for Pharmaceutical Applications

Master's thesis in Wireless, Photonics and Space Engineering

JOAKIM GARCIA WERNERSSON

Department of Microtechnology and Nanoscience
CHALMERS UNIVERSITY OF TECHNOLOGY
Gothenburg, Sweden 2015

THz Imaging of Roll Compaction for Pharmaceutical Applications

Joakim Garcia Wernersson

CHALMERS
UNIVERSITY OF TECHNOLOGY

Department of Microtechnology and Nanoscience
Terahertz and millimetre wave laboratory
Chalmers University of Technology
Gothenburg, Sweden 2015

THz Imaging of Roll Compaction for Pharmaceutical Applications
Joakim Garcia Wernersson

Supervisor: Alvaro Diaz-Bolado, AstraZeneca
Examiner: Helena Rodilla, Terahertz and millimetre wave laboratory

Master's Thesis 2015:NN
Department of Microtechnology and Nanoscience
Terahertz and millimetre wave laboratory
Chalmers University of Technology
SE-412 96 Gothenburg
Telephone +46 31 772 1000

Cover: Simulation setup for testing different samples using antenna simulations.

Gothenburg, Sweden 2016

THz Imaging of Roll Compaction for Pharmaceutical Applications Joakim Garcia Wernersson
Department of Microtechnology and Nanoscience
Chalmers University of Technology

Abstract

In the pharmaceutical industry, dry granulation is an intermediate state in the tablet manufacturing process for orally administered products. Powder blends with poor flowing properties are compressed and milled producing a granular material with increased flow properties. A key element in the process is the density of the compressed powder since it will affect the final quality of the manufactured tablet. The existing density measurement system employed by AstraZeneca is a destructive measurement.

This thesis shows a method for non-destructive density measurements using a terahertz imaging system. A model of the relation between the phase of the THz transmitted signal versus the permittivity of the sample was obtained through full-wave simulations using CST Microwave Studio. By determining the permittivity of samples with known density, a material specific model of how the permittivity varies with density was obtained.

The presented density control method has significantly decreased the measurement time by a factor of 2 and it is also capable of measuring the density over a 20 times smaller area of the sample compared with the method currently used at AstraZeneca.

Keywords: THz-imaging, density measurements, permittivity, CST simulation

Acknowledgements

This work would not have been possible without the preceding efforts and guidance of Robin Dahlbäck. I would like to thank my supervisors Helena Rodilla and Alvaro Diaz Bolado for their guidance and support. For the fantastic work environment and inspiration I would like to thank the staff of Terahertz and Millimetre Wave Laboratory.

I would like to Thank AstraZeneca for the opportunity to work on this thesis. Lubomir Gradinarsky, Håkan Wikström, Lien Nguyen och Mats Josefson for their guidance and instructions.

Finally, I wish to thank my girlfriend and family for their love and support through this master's program and thesis.

Joakim Garcia Wernersson, Gothenburg, April 2016

Contents

1
Introduction

Imaging in the Terahertz (THz) frequency region of the electromagnetic spectrum, usually defined as the region 0.3-3 THz corresponding to a wavelength of 1-0.1 mm, has received a lot of attention since the new millennium. Research and implementation has been made in fields such as, security screening [1], satellite systems [2], medical diagnostics [3] and pharmaceutical processes such as tablet coating thickness measurements as well as hardness measurements [4].

The THz region is placed between the microwave region and the visible spectrum. Using THz for imaging instead of microwave frequencies has the advantage of the proportional relation between resolution and wavelength. Moreover, the smaller wavelength also contributes to smaller components making the system more compact. While the visible region has an even smaller wavelength, its penetration depth is shallow, making most materials opaque. Most packaging material can be penetrated using THz imaging, making possible a non-invasive packages scanning without the need of X-rays.

This thesis is a collaboration between Chalmers and AstraZeneca to investigate the possibility to obtain the density and moisture content of a roller compacted paracetamol formulation using a THz-imaging system. With this method we aim to increase the efficiency and accuracy of the destructive method currently used in AstraZeneca.

1.1 Background

Roller compaction is a pharmaceutical process used in the pharmaceutical industry for dry granulation of moisture and heat sensitive powder blends with poor flowing properties. Dry granulation is an intermediate state in the tablet manufacturing for orally administered products. The Roller compaction process produces an agglomerate strip, 4 cm in width, which is often referred to as a ribbon. The ribbon is milled to produce a granular material with higher flow properties than the initial powder. The roller compactor used to fabricate the samples used in this thesis is an Alexanderwerk WP120. Alexanderwerk WP120 uses an horizontal screw to feed the powder to the compactor rolls. The speed of the rolls, feed and roll gap, will determine the density of the samples, see figure 1.1.

Key parameters of the roller compaction process are the moisture content and density of the ribbons since they will affect the final quality of the manufactured tablet. The current system used at AstraZeneca to measure the ribbon density is based on destructive measurements. The system measures the displacement of very

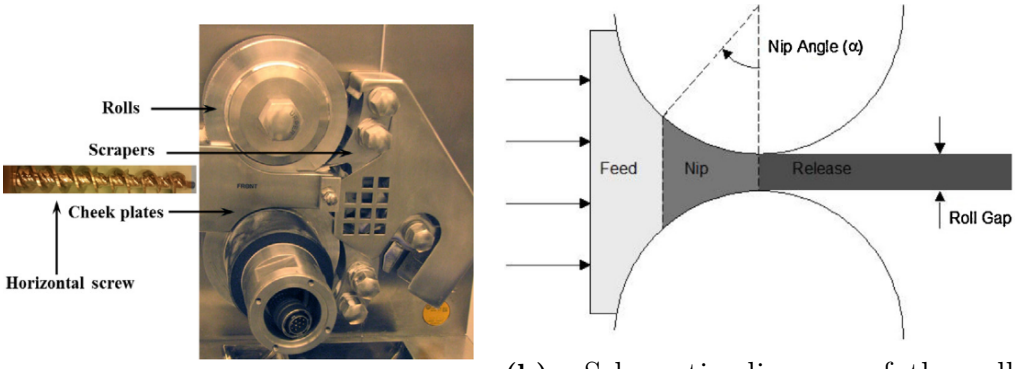

(a) Alexanderwerk Roller compactor **(b)** Schematic diagram of the roll compaction process

Figure 1.1: (a) Alexanderwerk roller compactor used to create flat and patterned ribbons. (b) Schematic view of how the powder is compressed between two rolls to create the ribbon. Controlling the roll gap, the speed of the rollers and the feeding speed, different densities are obtained. [5]

fine sand in a test tube, measuring with and without samples inside. One measurement takes up to 30 minutes and the result can depend on the person operating the measuring system. It is common to take several measurements for each sample under study, requiring a sample size of around 2 grams for each measurement. The finite size of the test tube requires the ribbon to be cut in squares of 10 by 10 millimeters. For maximum accuracy these squares should be taken from the center of the ribbon.

This thesis explores the possibility of using THz imaging for measuring the density of the ribbons. The system will perform non-destructive measurements and make use of the relation between the dielectric properties and density for a compressed powder material to determine the density of the samples. The effective permittivity of a compressed powder material is a mixture of the material and air, making the dielectric properties change with the density of the material.

1.2 THz-imaging

THz-imaging uses THz electromagnetic waves and the known signal path to obtain information of the materials in the signal path. There are two main configurations of THz-imaging systems: stand-off imaging and sample investigation system [16]. Stand-off imaging is used to observe a target from a distance, for example in satellite systems [2] and security screenings [7]. Sample investigation system is the system configuration used in this thesis and is characterized by the ability of moving and placing the samples inside the measuring system, making possible to have longer measuring and processing time.

THz-imaging may be used to investigate the dielectric properties and the shape of the samples. The dielectric properties of a material describe how the electromagnetic wave travels through the material and how much is attenuated. An electromagnetic wave suffers a change of wavelength when crossing a dielectric. This

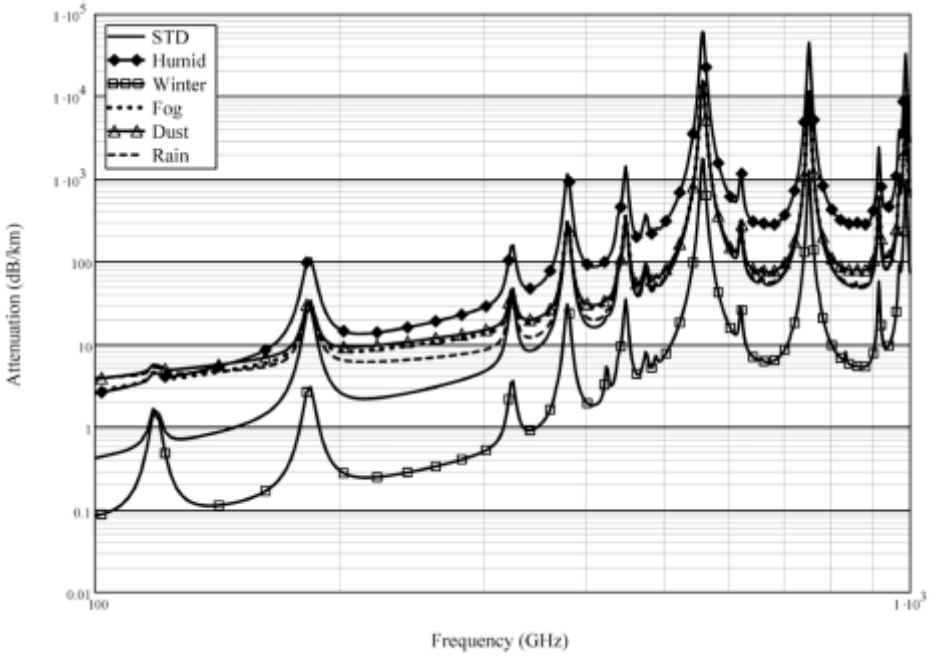

Figure 1.2: Atmospheric attenuation as a function of frequency in the range 100 GHz-1 THz for different weather conditions. [8]

change in wavelength is translated into a change in phase. Thus, measuring this change of phase will give insight into the dielectric properties of a material.

The attenuation of electromagnetic waves propagating in a medium is usually frequency dependent. An example can be observed in figure 1.2 were the atmospheric attenuation of electromagnetic waves with frequencies from 0.1 to 1 THz are plotted for different weather conditions. The lowest attenuation is in winter, when the humidity is low, and the highest attenuation occurs when the weather is humid. The difference between the two is for a majority of the frequencies is a factor of 100, showing that water is a highly absorptive liquid in the THz frequency range and has a large influence on the attenuation of a signal.

Since there is a large impact on the attenuation of a material due to water content, it is possible to measure the moisture content of a sample by measuring the power of the received signal.

1.3 Scope

The Aim of this thesis is to find a way to obtain the density and moisture content of ribbons using a THz-imaging system. The project shall use the system built by Robin Dahlbäck [6], and only make minor changes to the system if needed. The ribbons are made of a Paracetamol based formulation.

In this thesis, a permittivity model is created from simulation results and measurements. Priority is given to carry out the density measurement and further if there is time, consider the moisture content measurements.

1.4 Thesis Layout

Chapter 2 describes the permittivity properties of particulate materials and the theory of the relation between permittivity, density and moisture content. In *Chapter 3* the measurement system is explained as well as the samples used in the thesis. *Chapter 4* gives a description of how the measurements were done, simulations were carried out and how the models were constructed. *Chapter 5* Shows the results of the simulations, measurements and the model of how density relates to permittivity. Finally, *Chapter 6* presents the important conclusions and suggestions on further research and improvements.

2
Theory

2.1 Dielectric properties

The relative complex permittivity of a material is often denoted as:

$$\epsilon_r = \epsilon' - j\epsilon''$$

where ϵ' is the dielectric constant and ϵ'' is the dielectric loss factor. The dielectric loss factor is a measure on how much the material converts the electromagnetic energy into heat due to damping of the vibrating dipole moments [10].

The dielectric properties for low-loss dielectrics may be calculated by measuring the changes of phase and amplitude of a plane wave inside the dielectric [11]

$$\epsilon' = \left[1 + \frac{\Delta\phi}{360d}\frac{c}{f}\right]^2 \tag{2.1}$$

$$\epsilon'' = \frac{-20log(\frac{A_{meas}}{A_{freespace}})}{8.686\pi d}\frac{c}{f}\sqrt{\epsilon'} \tag{2.2}$$

where c is the speed of light, f is the frequency, d is the thickness of the material, $\Delta\phi$ is the change in the phase when compared to free space propagation, A_{meas} is the measured amplitude of the received signal and $A_{freespace}$ is the amplitude of the received signal if the sample was vacuum.

From Eq. (2.1) and (2.2) we observe that the real part of the permittivity can be obtained by observing the phase difference and thickness, while the imaginary part is determine by the loss in the dielectric and the real part of the permittivity.

The samples in this project are made from a compressed paracetamol formulation. In this case the effective permittivity is a combination of the permittivity of the paracetamol formulation and air. A sample compressed with a higher force will have a lower amount of air in it, making the effective permittivity higher.

As explained in the introduction, in this thesis we have studied the ability to obtain the density and moisture content by determining the permittivity from THz imaging.

2.2 Density - Permittivity relation

Empirical studies made by Stuart O. Nelson et al. [12] [13] [14], suggest that there is a linear relation between the density of granular materials and their permittivity:

$$\rho = \frac{a_f \epsilon' - \epsilon''}{a_f k} \tag{2.3}$$

where a_f and k are constants dependent on the material and frequency and ρ is the material density.

The frequency in this thesis is fixed at 346 GHz.

2.3 Permittivity - Moisture content relation

The study by Trabelsi et al. [15] shows that the relation between moisture content and permittivity can be described independent from the density, for a fixed material and frequency, using the expression:

$$\Psi = \sqrt{\frac{\epsilon''}{\epsilon'(a_f \epsilon' - \epsilon'')}}$$

where a_f is constant for a given frequency and material. Ψ is proportional to the moisture content in percent. Using linear regression on the form:

$$\Psi = A \cdot M + B$$

where M is the moisture content in percent, A and B are frequency and temperature dependant constants, it is possible to extract the material specific moisture content.

2.4 Propagation in discontinued media

This section will describe how the permittivity affects the propagation of an electromagnetic wave, used as a simplified model of what will be measured by the THz-imaging system.

Consider a uniform non-magnetic sample infinite in two dimensions with a finite thickness d, surrounded by air, see figure 2.1. How electromagnetic waves propagate through the sample, assuming uniform plane waves, can be described by the propagation matrix defined as:

$$\begin{bmatrix} E'_{2+} \\ E'_{2-} \end{bmatrix} = \begin{bmatrix} e^{jkl} & 0 \\ 0 & e^{jkl} \end{bmatrix} \begin{bmatrix} E_{2+} \\ E_{2-} \end{bmatrix} \tag{2.4}$$

Where k is the wave-vector, $k = \omega\sqrt{\mu_0(\epsilon' - j\epsilon'')\epsilon_0}$, l is the distance the wave travels through the sample and j is the imaginary unit. E_{2+} is the electric field at incident and E'_{2+} is the electric field after it has propagated l distance in the positive direction, analog for E_{2-} and E'_{2-} in the negative direction.

When electromagnetic waves propagate through a boundary between different mediums, the waves will be partly reflected while the rest will be transmitted. The reflectance and transmittance caused by the change of material can be described by the matching matrix [9]:

$$\begin{bmatrix} E_{1+} \\ E_{1-} \end{bmatrix} = \frac{1}{\tau_{12}} \begin{bmatrix} 1 & \rho_{12} \\ \rho_{12} & 1 \end{bmatrix} \begin{bmatrix} E_{2+} \\ E_{2-} \end{bmatrix} \tag{2.5}$$

where ρ is the reflectance and τ the transmittance calculated using Fresnel's formulas for normal incidence:

$$\rho_{12} = \frac{n_1 - n_2}{n_1 + n_2} \qquad \tau_{12} = \frac{2n_1}{n_1 + n_2} \tag{2.6}$$

where n_1 and n_2 is the refractive index of the different mediums. The refractive index can be expressed in permittivity as $n = \sqrt{\epsilon_r}$ for a non magnetic medium.

How the sample surrounded by air affects a plane electromagnetic wave is described by combining Eq. 2.4 and 2.5 into:

$$\begin{bmatrix} E_{1+} \\ E_{1-} \end{bmatrix} = \frac{1}{\tau_{12}\tau_{23}} \begin{bmatrix} 1 & \rho_{12} \\ \rho_{12} & 1 \end{bmatrix} \begin{bmatrix} e^{jkl} & 0 \\ 0 & e^{jkl} \end{bmatrix} \begin{bmatrix} 1 & \rho_{23} \\ \rho_{23} & 1 \end{bmatrix} \begin{bmatrix} E_{3+} \\ E_{3-} \end{bmatrix} \tag{2.7}$$

where ρ_{12} and τ_{12} is the reflectance and transmittance of the first boundary from air to sample. ρ_{23} and τ_{23} is the reflectance and transmittance of the second boundary from sample to air. Assuming that the sample is illuminated from the left ($E_{3-} = 0$), the reflection coefficient Γ and the transmittance coefficient T for the sample are:

$$\Gamma = \frac{E_{1-}}{E_{1+}} \qquad T = \frac{E_{3+}}{E_{1+}} \tag{2.8}$$

In this thesis we will consider samples of different densities and thereby different permittivities in order to find a relation between the two. The theoretical relation between permittivity, thickness and phase difference can be calculated using Eq. 2.7, see figure 2.2. The figure suggest an observable difference in phase with different thickness and permittivity, while the amplitude of the transmittance is not uniquely determined.

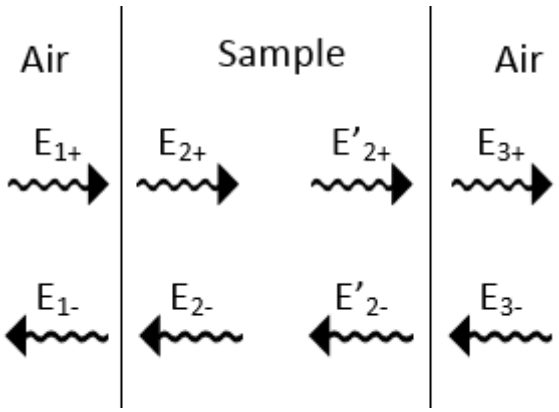

Figure 2.1: Figure depicts how the boundary of discontinued mediums affect a propagating wave. E_{1+} is the incoming wave and E_{1-} is the reflected wave when the medium changes from air to sample. E_{2+} is the transmitted wave and E'_{2+} is the wave after propagating through the sample. E_3+ is the transmitted wave while E'_{2-} is the reflected wave when changing medium from sample to air. The sample is only illuminated from the left, thus making $E_{3-} = 0$

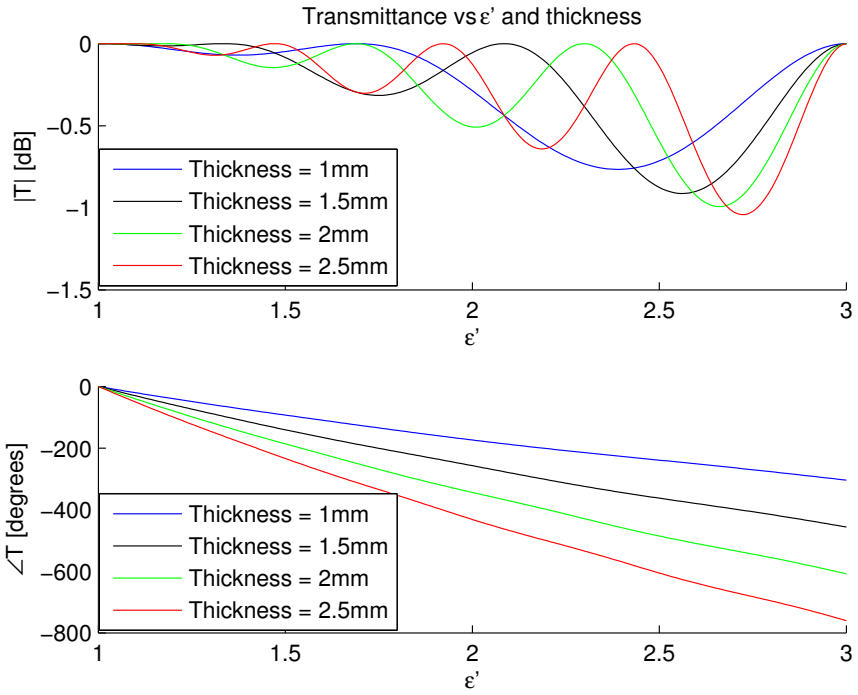

Figure 2.2: Simulated transmittance of an infinite lossless sample using plane waves when varying the thickness and real part of the permittivity.

3

Setup and Samples

This Chapter will give an overview of the used THz-imaging system and the measured samples. For a more in-depth explantion on the system, the reader is referred to Robin Dahlbäck's original thesis [6] and article [16].

3.1 The Measurement System

The imaging system consists of an emitter and a receiver, each having one antenna. The antennas are open-ended rectangular waveguide probes and are placed 7.97 mm from each other. The setup is a continuous wave (CW) system, meaning that the transmitting antenna is constantly transmitting. In this thesis, the frequency used is 346 GHz.

The system uses up-conversion from microwave frequencies for the emitter and sub-harmonic mixers for detection. The system is driven by two CW sources, a low frequency synthesizer operating at 912 MHz and a high frequency synthesizer operating at 34.6 GHz, see figure 3.1. The synthesizers create both the transmitted signal and the LO-drive signal for the receiver side making them phase correlated and thus reducing measurement noise [16].

The received signal is down-converted to a DC signal using an I-Q demodulator which is amplified and detected in the data acquisition system. From the I and Q signals, both the phase and the amplitude of the signal can be extracted.

In order to measure the sample at multiple positions with high precision, the setup is mounted onto a 4-axis mechanical setup, see figure 3.2. Note that the imaging region is between the two antenna probes. The antenna probes move independently of each other perpendicular to the propagation direction in x and y direction, as illustrated in figure 3.1.

The sample is placed between two polycarbonate plates situated on a hard plastic holder and fastened by plastic screws. The sample holder is placed between the two antennas. To minimize transitions between different mediums, there is an opening through the polycarbonate so the only medium transitions are the air-sample transitions, see figure 3.3 and 3.4. Further advantage of the opening is that polycarbonate is a bendable material and the curvature of the polycarborate will then create diffraction at different angles over the sample.

The distance from the receiver to the holder is fixed at 2.3 mm, while the distance from the sample to the transmitter differs with the thickness of the sample.

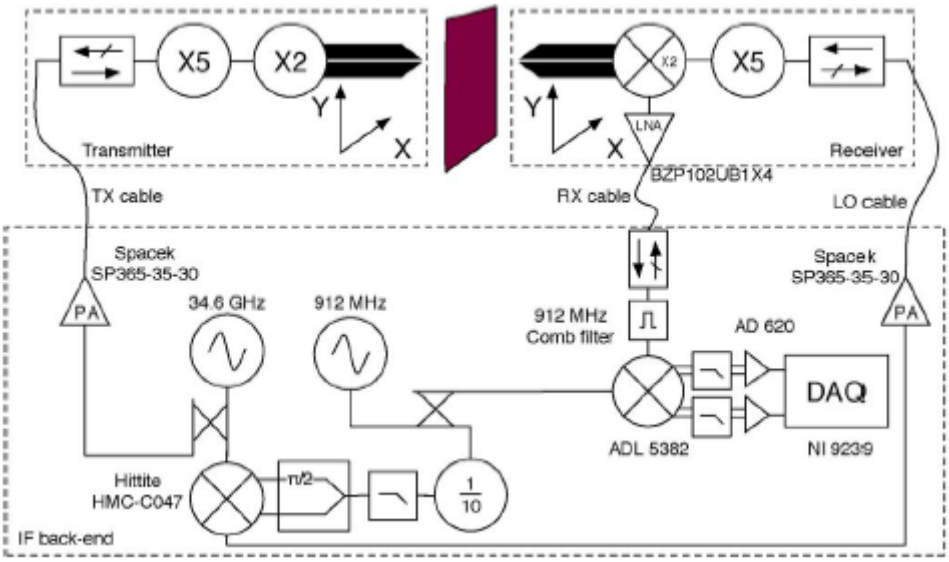

Figure 3.1: Block diagram showing the electronics of the THz-imaging system [16].

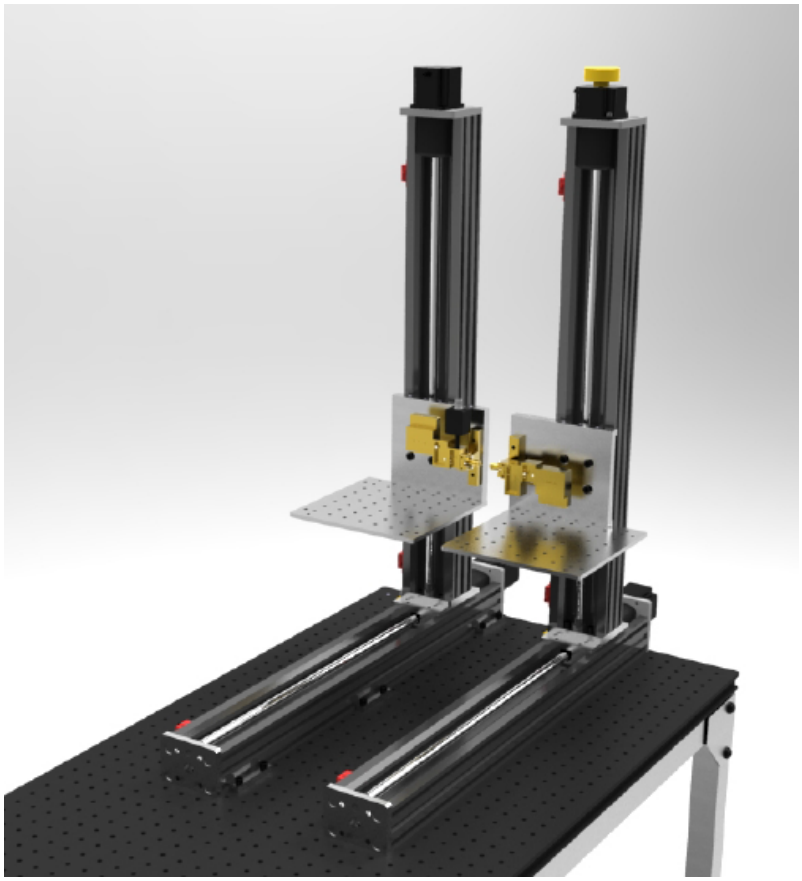

Figure 3.2: The figure shows the 4-axis mechanical system with the setup mounted to it. Note that the imaging region is between the two probes [6]

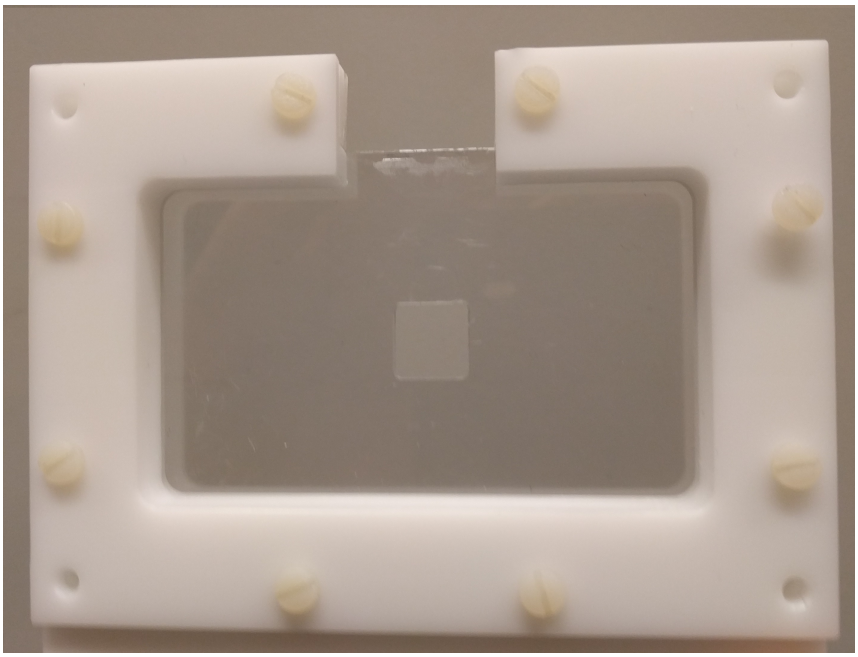

Figure 3.3: Image of the sample holder empty. The opening can be observed in the center of the holder.

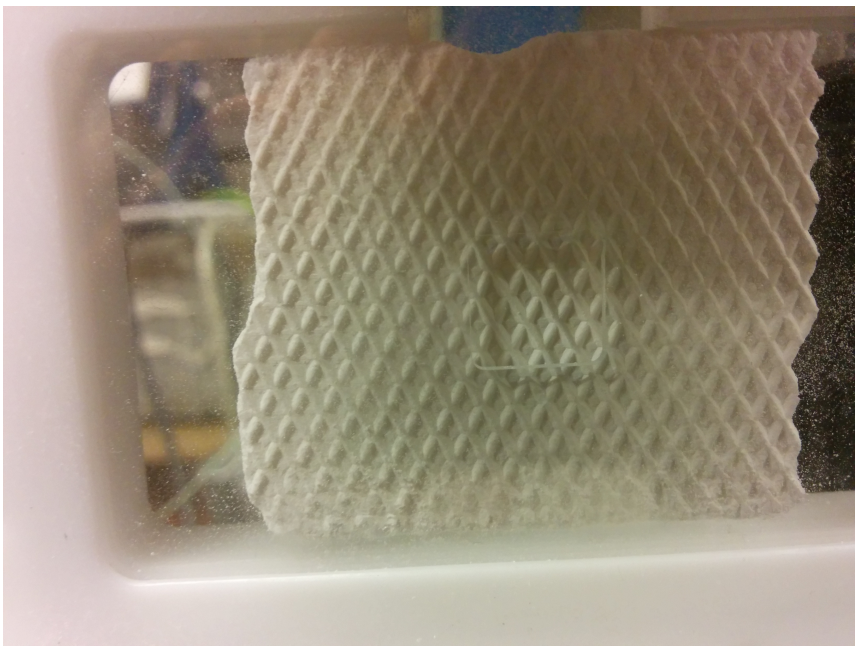

Figure 3.4: Image of the sample holder loaded with a patterned sample.

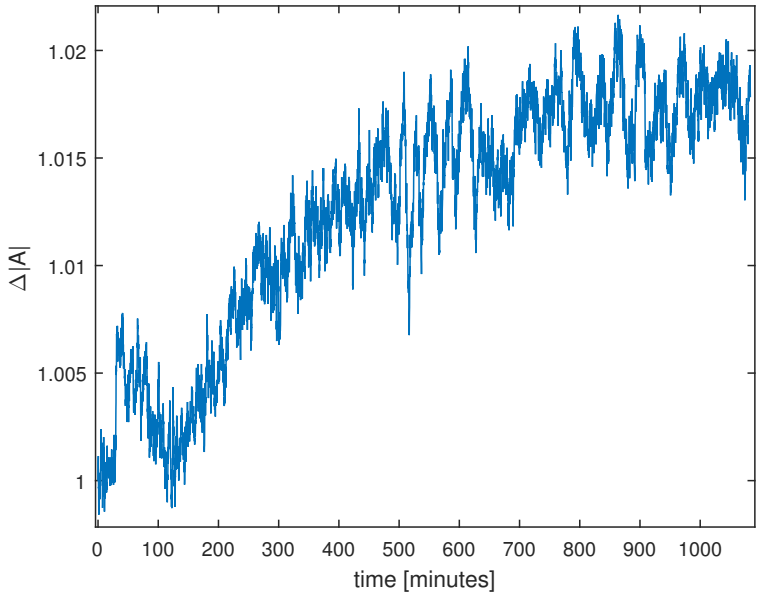

Figure 3.5: Performance measurement without sample and fixed antennas. A measurement is taken every 10 s over the course of a day. The amplitude is normalized with regards to the initial measurement.

3.2 Performance test

In order to test the measurement system over time, a performance test was made by removing the sample holder, keeping the antennas fixed, and measuring every 10 seconds over the course of a day. Figure 3.5 shows the variation of the amplitude of the received signal over a day, which is slightly drifting by less than 2%. The performance of the system is stable over a short time frame of one hour with a maximum change of 1%. Figure 3.6a shows the phase difference from the same measurement, figure 3.6b shows the difference when zoomed in. Note that there is a periodicity to the fluctuations of approximately 30 minutes. This could be due to temperature fluctuations due to the air conditioning turning on and off. The phase difference in 15 minutes is approximately 4.5 degrees. Between 100 and 400 minutes, see figure 3.6a, there is a drift in the average received phase of approximately 3 degrees. Since there is a drift over a few hours, there is a need to recalibrate the system before each measurement. Since one measurement with calibration and reference measurement can take over 15 minutes, the estimated error in the phase due to the setup is $\pm 5°$.

3.3 Samples

All samples were produced at AstraZeneca. The samples consist of paracetamol as the active drug and a number of non-therapeutic compounds which are called excipients. The excipients are typically used for immediate release tablets [5]. In this thesis, three kinds of samples were studied: flat ribbons, patterned ribbons and

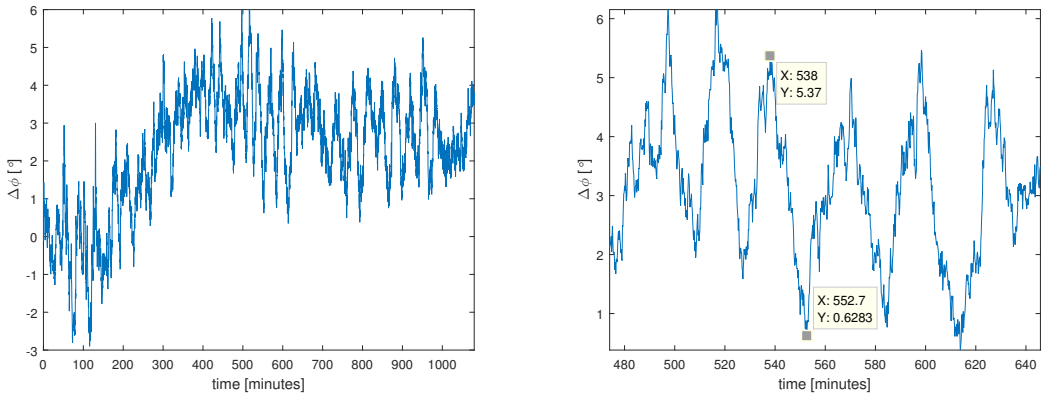

(a) Whole day measurement **(b)** Zoomed in measurement

Figure 3.6: Performance measurement without sample and fixed antennas. (a) A measurement is taken every 10 s over the course of a day. The phase difference is taken with regards to the first measurement. (b) Same measurement as (a) zoomed in, note the phase difference of 4.75 degrees over ≈15 minutes, which is comparable to the measurement time of one sample.

tablets, see figure 3.7.

3.3.1 Sample requirements

The samples need to fit inside the sample holder. This will mainly restrict the thickness of the samples, but also the width and height of them. The samples also need to be of sufficient thickness. A too thin sample causes insufficient change in phase and amplitude for different densities, making the uncertainty of ±5° have a strong influence on the results. A too thick sample can cause problems due to phase ambiguity, were determining the number of periods is impossible.

3.3.2 Tablets

The tablets were made by compressing a powdered paracetamol formulation into a cylindrical shape at AstraZeneca. The radius of the tablets can be considered constant at 10.1 mm. Different densities of the tablets were achieved through regulating the compressing power of the setup using approximately the same amount of powder in all tablets. The difference in compressing power made the height of the cylinder different for the different samples, and consequently the densities of the samples were different, see table 3.1. There were 3 tablets for each of the 3 different densities. The tablets were mainly used for preliminary measurements. Due to their size they proved difficult for the THz-imaging system to measure.

3.3.3 Patterned Samples

The samples used were compressed using an Alexanderwerk WP120 roll compactor. Alexanderwerk WP120 uses a horizontal screw to feed the powder to the compactor

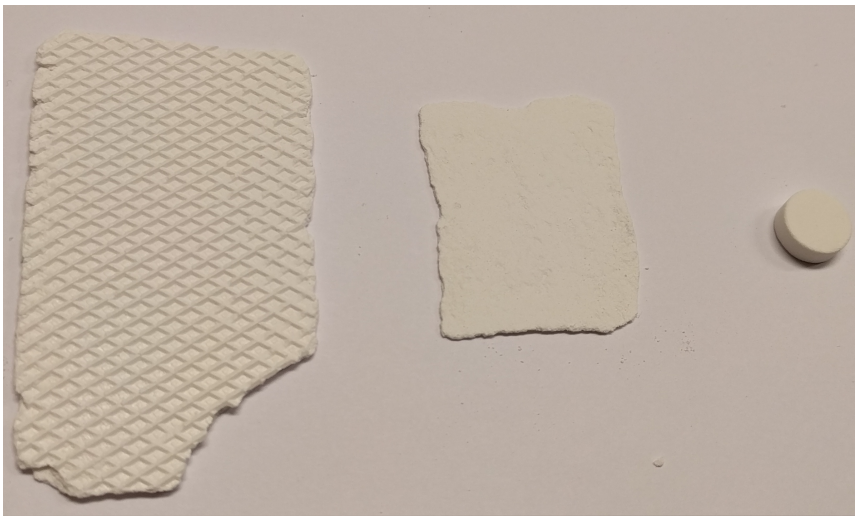

Figure 3.7: The figure displays the three different samples used in this thesis. Patterned sample to the left, flat sample in the middle and tablet to the right.

tablet	diameter[mm]	thickness[mm]	weight[mg]	density[g/cm^3]
low1	10.118	3.748	293.5	0.9739
low2	10.115	3.748	291.3	0.9672
low3	10.115	3.751	293.8	0.9747
med1	10.100	3.285	299.1	1.1364
med2	10.097	3.281	294.8	1.1221
med3	10.097	3.279	290.6	1.1068
high1	10.082	3.053	301.9	1.2387
high2	10.086	3.020	299.6	1.2417
high3	10.079	3.060	308.7	1.2644

Table 3.1: The table shows the different parameters of the tablets used for testing.

rolls. The speed of the rolls, feed and roll gap will determine the density of the samples. The patterned samples, see figure 3.7, are flat on one side and patterned on the other. The pattern consist of half cylinders with a radius of 0.35 mm that intersect at 60° and 120°. This shape is due to one of the rolls having the pattern in order to increase the friction coefficient between the powder and the roll [5].

3.3.4 Flat samples

Flat samples are made from patterned samples that have split in the roller compactor by sticking to the rolls and being scraped off by the scrapers. Splitting creates a roughness to the surface, making impossible to measure their exact thickness using a micrometer. For this thesis, both the flat samples created by the roller compactor and the patterned samples were treated with sandpaper in order to create a smooth surface.

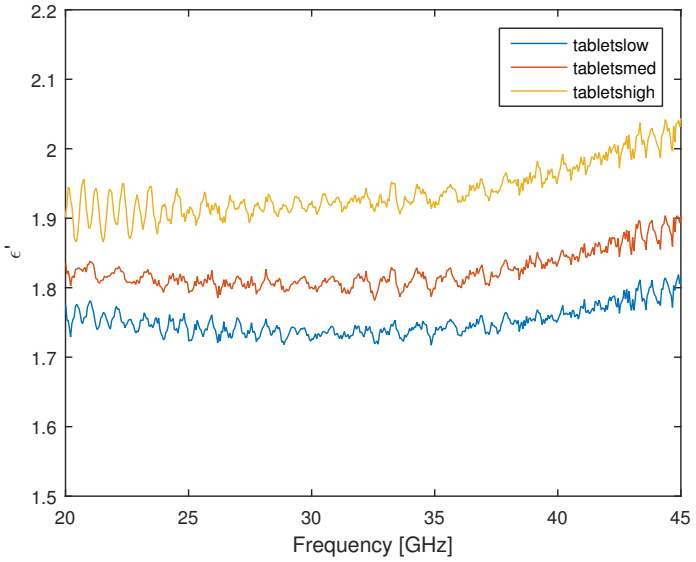

Figure 3.8: Plot of ϵ' for three different tablets of different densities. Results from measurements performed at AstraZeneca with an Agilent 85070E Dielectric Probe Kit to determine the real part of the permittivity. Tablets of Low, medium and high densities corresponding to 0.97, 1.12 and 1.24 g/cm^2.

3.3.5 Preliminary measurements

Initial measurements of the permittivity of the tablets were made by me at AstraZeneca in order to ensure that the difference in density of the samples under study was translated into a detectable change of permittivity. The permittivity was measured with an Agilent 85070E Dielectric Probe Kit. The setup consisted of a Vector Network Analyser (VNA) measuring from 0 to 50 GHz, connected to a open coaxial probe where the samples were placed. This setup is mainly intended for characterizing liquids and was calibrated using water, air and acetone. The sample is placed in contact with the open coaxial probe. The permittivity is then extracted from the reflection coefficient measured using the VNA.

The setup assumes that there is an infinitely long sample after the probe, therefore tablets of the same density were stacked on top of each other to increase the effective thickness. Figure 3.8 displays the obtained ϵ' variation due to different tablets in the range 20-45 GHz. The figure shows a distinct difference in permittivity for the different densities, even if the measurement is done at a lower frequency than the THz measurements later, this is a good indication that there will be a detectable change of permittivity for higher frequencies as well. To determine the densities of the tablets, they were weighed and measured under the assumption that they were perfect cylinders, the results can be seen in table 3.1

The obtained values of ϵ'' were in the order of 0.1 with low difference between the different densities. For this reason, ϵ'' was assumed to be constant at 0.1 in this study. This entails that there is only need to determine the ϵ' for the permittivity-density relation, which can be obtained by measuring the phase and thickness of the samples.

4
Method

This chapter describes how the density is obtained from simulations and measurements of the phase and thickness of the samples. The chapter also describes how the simulations are used to construct models of permittivity and density.

4.1 Simulations

The THz imaging setup was simulated using a full-wave commercial simulator, CST Microwave Studio, since the shape of the samples and sample holder make analytical calculations of diffraction and scattering difficult. The simulations were carried out to understand the dependence of the sample size and dielectric properties on the received signal. The simulation data is then used to create a model that relates the received phase of a measurement to the permittivity of the sample for a given sample thickness.

4.1.1 Infinite sample

As a first approximation, an infinitely large sample surrounded by vacuum and illuminated by a plane wave was simulated, see figure 4.1a. A reference simulation is done by substituting the sample material by vacuum, making possible to observe the phase difference caused by the sample. The phase difference is only influenced by the thickness and permittivity of the sample.

This first approximation of plane wave with no holder was compared with a simulation with plane wave but in this case with a sample holder. In this way the influence of the holder in the measurements can be studied.

4.1.2 flat sample in holder

The sample now placed in a holder made from polycarbonate with a square shaped hole in the middle, see figure 4.1b. The size of the hole is 10 by 10 millimeter with rounded edges.

By comparing the simulation with and without sample in the holder it is possible to find the phase difference of the received electric field, see figure 4.2. There will be an added disturbance due to edge diffraction from the hole in the polycarbonate plates.

By averaging the phase difference with and without a sample inside the holder, taken from the measurement region in the center of the holder, it is possible to

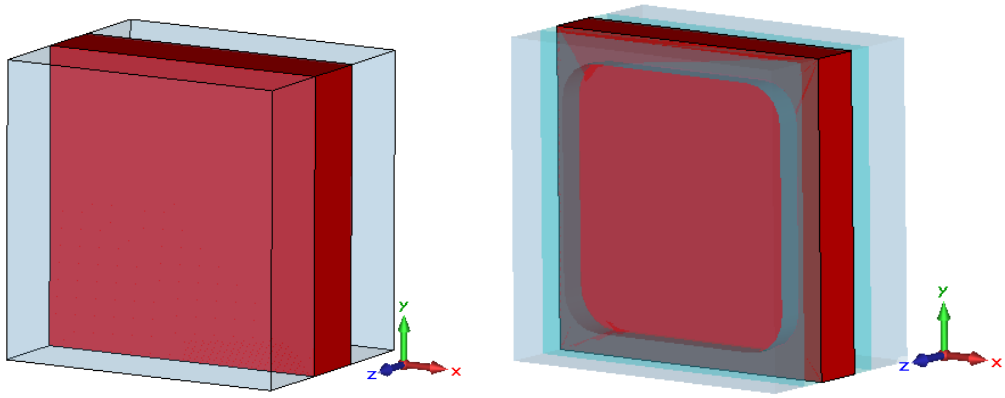

(a) Infinite sample in free-space **(b)** Flat Sample in holder

Figure 4.1: Simulation setup for different samples in free-space as well as when samples are put inside a holder. The simulations are done using plane waves with the propagation direction being in positive z

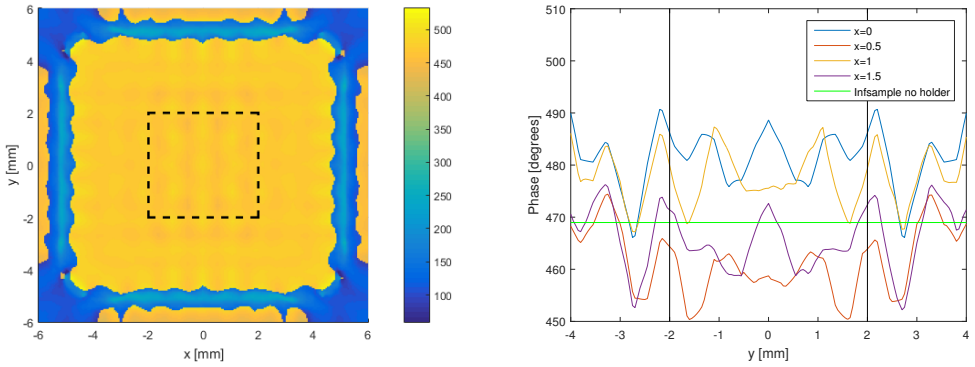

(a) Flat sample in holder **(b)** cut along y-axis

Figure 4.2: a) The plot to the left shows the simulated received E-field from a flat sample placed in the holder with thickness 1.8 mm and $\epsilon' = 2.5$. The colorbar indicates the angle in degrees. The black dashed line indicates the measuring region. b) The figure on the right shows cuts from the left figure for fixed x values, the black lines indicate the measuring region

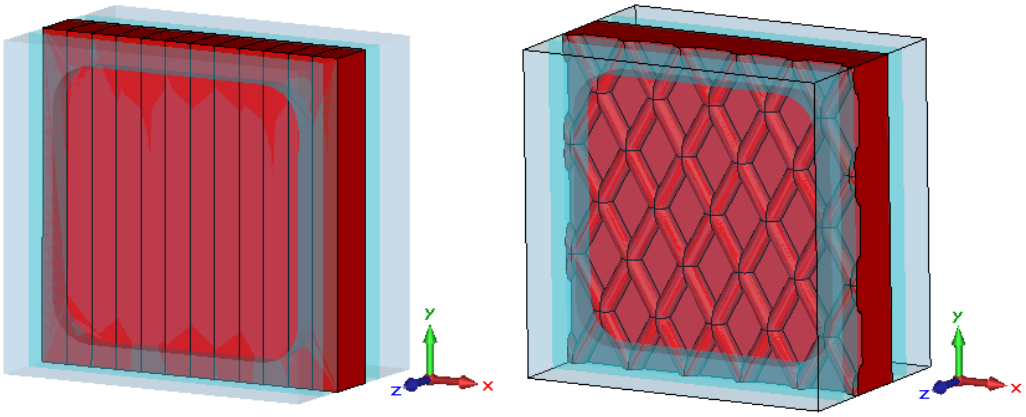

(a) Flat sample with varying density **(b)** Patterned sample in holder

Figure 4.3: Simulation setup for different samples inside a holder. The simulations are done using plane waves with the propagation direction being in positive z

remove all the effects of the holder and only leave the effects of the sample. Figure 4.2 shows a typical received E-field and the dashed region represent the measurement region of 4x4 mm. Note that the edge diffraction causes the phase to vary in the measurement region approximately 50°.

There is a possibility that the density varies over the sample's measured area. A simulation was carried out using a flat sample to see how the phase difference with and without sample varies if the permittivity changes every millimeter. See figure 4.3a for the simulation setup.

4.1.3 Patterned sample in holder

The patterned sample is the most common type of ribbon produced by AstraZeneca, and was a cause for concern in this project. As observable in figure 3.4 and 4.3b, the pattern consists of half cylinders cutting into each other at 60° and 120°. The pattern is the same in all the samples regardless of thickness. The pattern is made by half cylinders with a radius of 0.35 mm, spaced 2 mm apart from each other. The patterned sample is assumed to have a homogeneous density.

As in the previous simulations using flat samples, the phase is averaged over a measurement region of 4x4 mm in order to get rid of the effects of the holder.

Simulations of how the phase changes with varying displacement in x-direction and rotation around the z-axis were done in order to investigate the effect of possible misalignment when placing the sample in the holder.

4.1.4 Simulation using Antennas

The previous simulations were carried out using plane waves. This simulation uses antenna simulations and was carried out in order to see if the simulations using plane waves was a valid assumption. The distance from the transmitting antenna to the sample varies, with the smallest distance being ≈2 mm. The Fraunhofer criterion

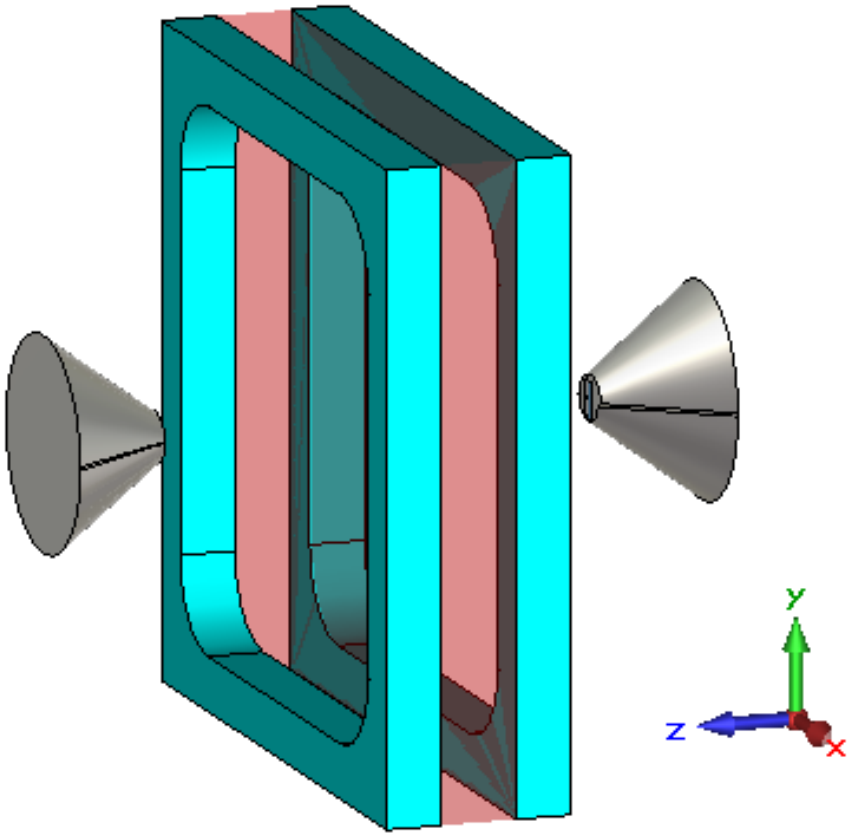

Figure 4.4: The simulation setup using antenna simulation with the propagation direction being in positive z

states the distance from the antenna to the far-field region is

$$r \geq 2D^2/\lambda$$

where D is the the largest dimension of the antenna and λ is the radiated wavelength. The calculated distance to the far-field region is $r = 1.17$ mm, satisfying the criterion for far-field. The rule of thumb for plane waves is $r >> \lambda$, which is not fully satisfied with $r \approx 3\lambda$ in this case. Due to the time required for the simulations, this was only simulated for flat samples, see figure 4.4. When simulating with antennas the thickness values were chosen from the samples that were experimentally measured.

4.2 Measurements

Measurements of the samples were carried out using the setup described in section 3.1. The measurement system measures the amplitude and phase of the received signal. The samples thickness were measured using a micrometer. The system is calibrated by blocking the antennas using an absorber in between the antennas to remove the leakage in the system. The measurements were taken over an area of 4 by 4 mm in the center of the sample and with a space between measurements of 0.2 mm. The total amount of sample points is 441 for each sample.

The measuring time for one sample point is 0.6 s, if time to move the antennas is included, the measuring time is between 4 to 5 minutes for each sample. The time for an empty holder reference measurement, moving the antennas away to access the sample holder as well as placing the sample inside the holder takes up to 20 minutes.

Placing the patterned samples inside the holder was carried out with caution to ensure the pattern alignment with the holder.

For a few samples measurements were taken at different parts of the ribbon to investigate if there was a change in density over the ribbons.

4.3 Constructing Models

This section will describe how the different models will be constructed. Figure 4.5 shows a flowchart of how the models are related.

4.3.1 Permittivity Model

The simulations were used to make a model for how the received angle depends on the thickness of the sample and the permittivity. From this model it is possible to extract how the permittivity depends on the measured received angle for a known sample thickness. Matlab was used in order to find a polynomial model for the permittivity with a multivariable least mean square fit.

$$\Delta\phi = p_{00} + p_{01}\epsilon' + p_{10}d + p_{20}d^2 + p_{11}d\epsilon' \implies$$

$$\implies \epsilon' = \frac{\Delta\phi - p_{00} - p_{10}d - p_{20}d^2}{p_{01} + p_{11}d} \tag{4.1}$$

where ϵ' is the real part of the permittivity, $\Delta\phi$ is the change in phase (degrees) when comparing the measurement with and without sample in the holder and d is the thickness of the sample. p_{xx} are the constants that works as weighting functions for the different parameters.

4.3.2 Density model

The density model will show the relation between the permittivity and the density of the samples.

By applying the permittivity model on the measured phase and thickness values, the permittivity of samples with known densities is obtained.

According to section 2.2 the relation between the permittivity and the density is linear. Therefore, the density model is constructed by doing a linear regression with an ordinary least squares estimation on the density and permittivity values.

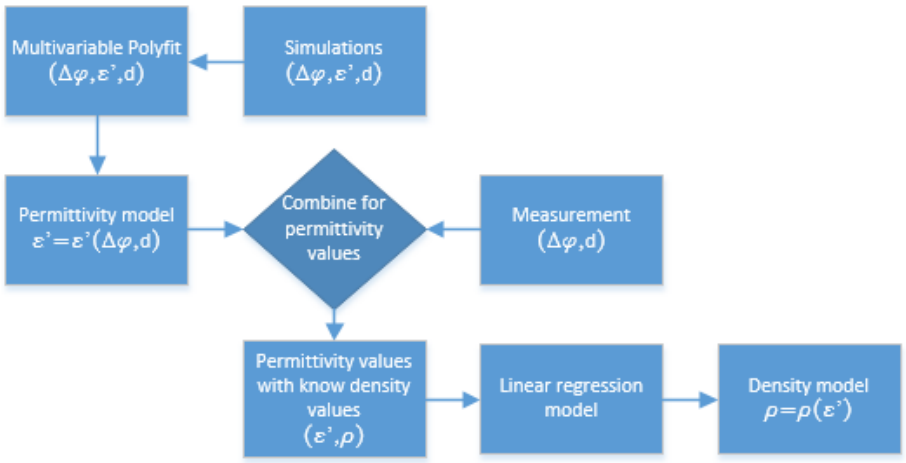

Figure 4.5: Flowchart of how the models are constructed and related

5
Results and Discussion

This chapter will present the results from the simulations described in the previous chapter. Permittivity and density models will be presented, as well as an analysis on the measurement errors.

5.1 Simulation Results

This section will present the simulation results used in the construction of the permittivity models. The simulations originally used lower permittivity values as measured in section 3.3.5, they were later re-simulated for values between 2 and 3, after the initial measurements indicated higher permittivity.

5.1.1 Infinite sample

The simulation results for plane waves and infinite sample are displayed in figure 5.1. Note that for a fixed thickness the phase difference with and without sample will be proportional to the permittivity of the sample. When varying the thickness, the slope changes.

5.1.2 Flat Sample in holder

The simulation results for flat samples in a sample holder illuminated with plane waves are displayed in figure 5.2. Note that the slope changes with the thickness of the sample.

A comparison of the phase difference between infinite flat sample in vacuum $\Delta\phi_{noholder}$ and flat sample in holder $\Delta\phi_{holder}$ show a negligible difference, confirming that by observing the average phase difference with and without sample in the measurement region the effects of the holder can be removed.

Figure 5.3 shows one simulation where the ϵ' increases 0.05 every millimeter in x-direction. The received E-field's phase over the measured area now increases when observing further along the x-axis. The rate of the increase depends on how much the density varies over the measured area as well as the thickness. By using the averaging method, the calculated permittivity will be the average permittivity over the measured area.

The simulation result of the flat infinite sample using simulated antennas is displayed in figure 5.4. When simulating with antennas instead of plane waves, the thickness values were chosen from the samples that were measured experimentally.

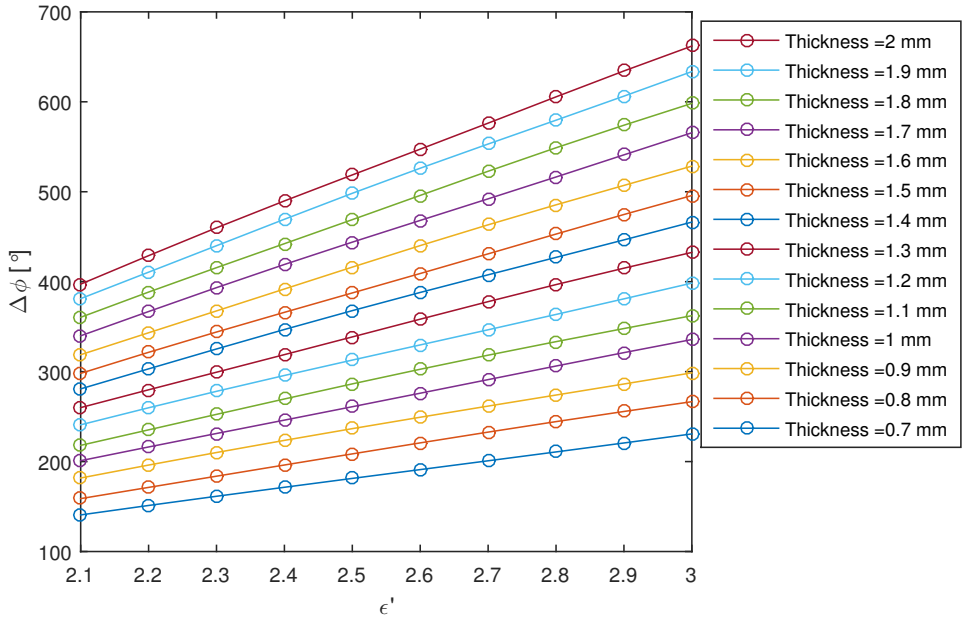

Figure 5.1: The plot depicts the simulated phase difference with and without a flat sample surrounded by vacuum under plane waves assumption. Samples with different ϵ' and thickness were simulated.

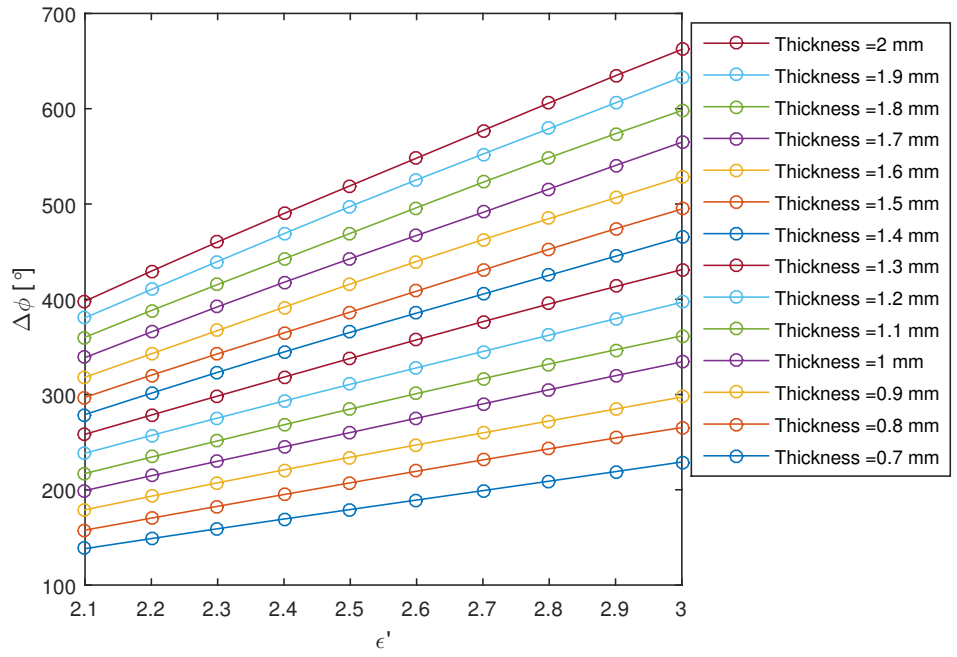

Figure 5.2: The plot depicts the simulated phase difference with and without a flat sample in the holder under plane waves assumption. Samples with different ϵ' and thickness were simulated.

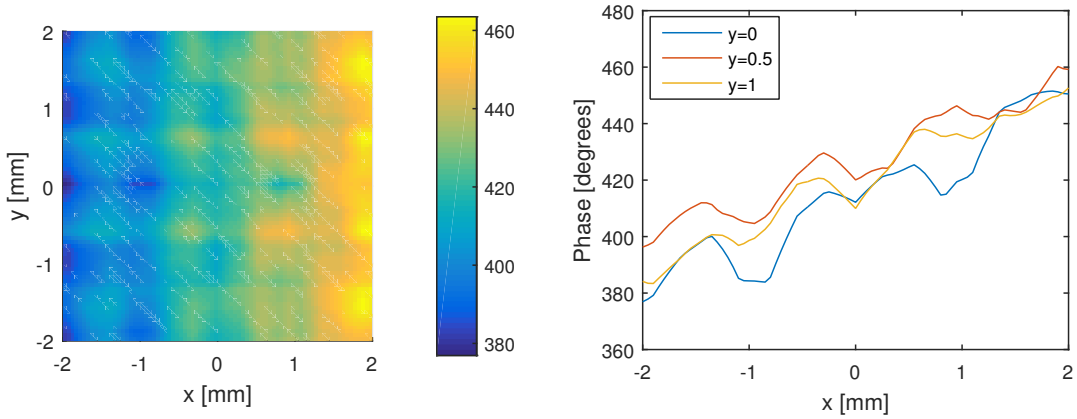

(a) Density varying flat sample

(b) cut along y-axis

Figure 5.3: The figure to the left shows the simulation results when the density varies along the sample. ϵ' varies in x direction 0.05 per millimeter. The colorbar represent the phase in degrees. The sample is 2 mm thick and $\epsilon' = 2$ at x=0. The figure to the right shows cuts from the left figure for fixed y values.

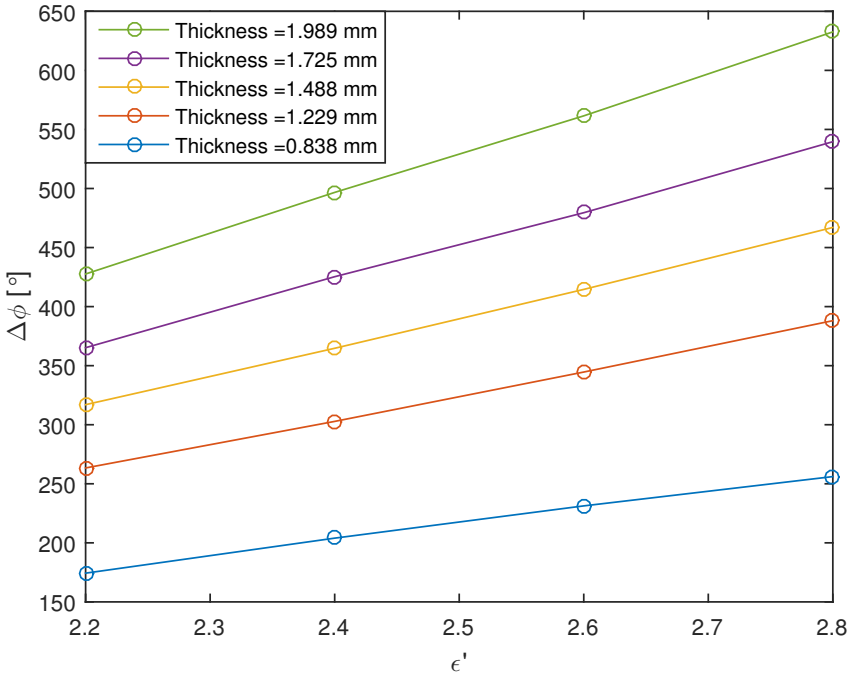

Figure 5.4: The plot depicts the simulated phase difference with and without a flat sample in the holder using the simulation with antennas. Samples with different ϵ' and thickness were simulated.

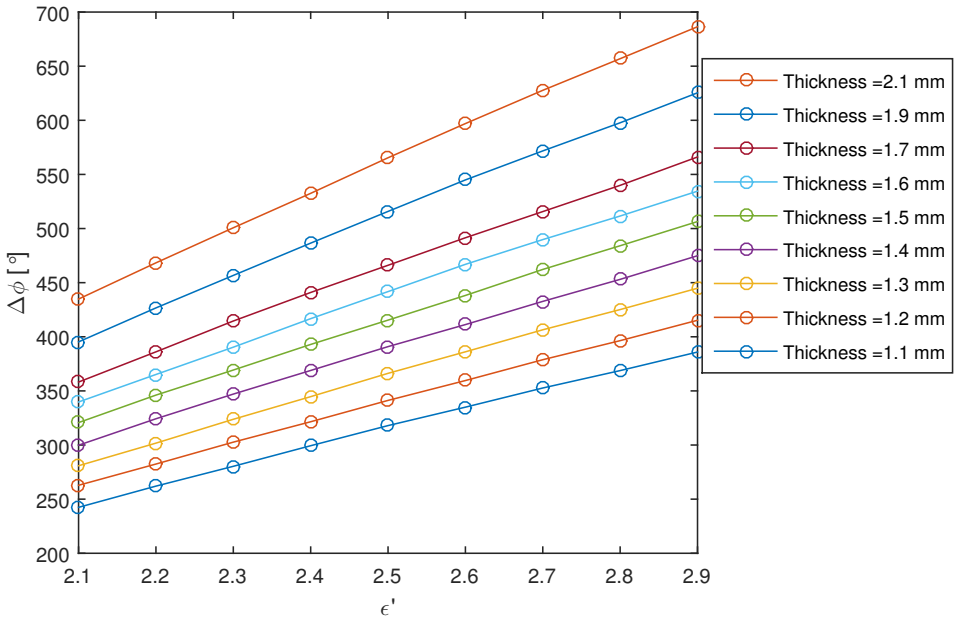

Figure 5.5: The plot depicts the simulated difference in angle between the results with a patterned sample and with the empty holder for different values of ϵ' and thicknesses

5.1.3 Patterned Sample in holder

The simulations of the patterned samples were carried out in accordance with the explanation presented in section 4.1.3. The simulation results of how the phase changes with permittivity and thickness of the samples are displayed in figure 5.5. Note that the slope of the graph depends on the thickness of the sample. When comparing the figure to the case of a flat sample, fig. 5.2, there is noticeable difference in the slopes for the different thicknesses.

Due to the pattern, the positioning of the samples in the holder affects the received signal. The alignment can be difficult so the pattern can be translated and rotated inside the holder. The effect of translation and rotation is significant, see figure 5.6. Translation as small as 0.2 mm results in a change in the average received phase of 8°, see figure 5.6a. Rotations of 1° around the propagation axis may also cause the average received phase to change 8°, see figure 5.6b.

Figure 5.7 displays the phase difference with different radius of the pattern cylinders. Note the phase difference from a radius of 0.35 to 0.25 mm is a minimum of 20° depending on the permittivity of the sample. This is an important result that shows that a potentially damaged pattern will have a significant impact on the received phase.

5.2 Constructing the permittivity models

The simulated values of thickness, permittivity and received phase were used to make a multivariable polynomial fit, see Eq. 4.1.

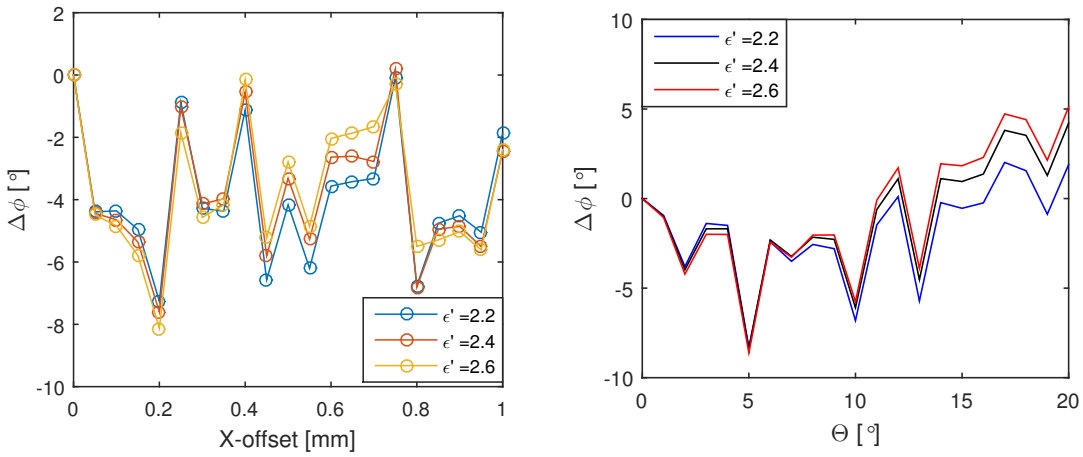

(a) Translated sample

(b) Rotated sample

Figure 5.6: The plot to the left depicts the simulated average phase change when the patterned sample is moved in the x-direction. Simulated for a sample thickness of 2 mm and three different permittivity values(2.2, 2.4 and 2.6). The plot to the right depicts the average phase change when the patterned sample is rotated Θ degrees around the z-axis. Simulated for a sample thickness of 2 mm and for different ϵ'.

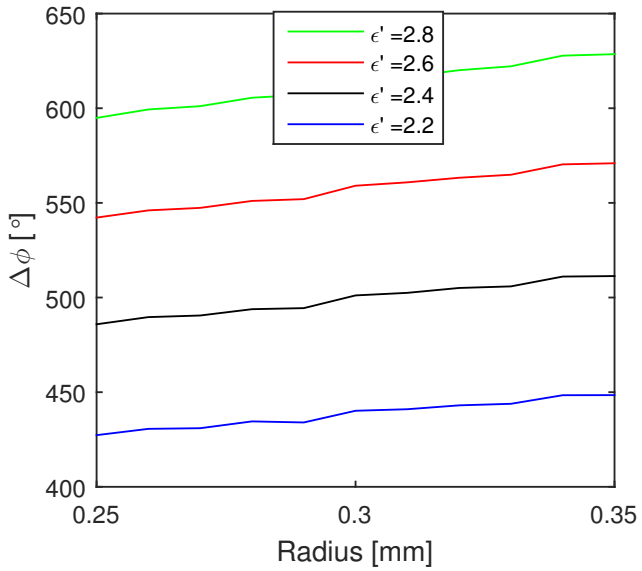

Figure 5.7: The plot depicts the simulated average phase change when the ”cylinders” of patterned sample changes radius. Simulated for a thickness of 2 mm and different permittivity.

Table 5.1: The table shows the different parameters for the permittivity model, when simulating the received phase under plane wave assumption and antenna simulation.

parameter	plane waves flat	antenna simulation	plane waves patterned
p_{00}	-4.636	22.01	-121.3
p_{01}	0.1961	-9.225	56.53
p_{10}	-105.6	-179.3	-5.366
p_{20}	-0.03016	4.448	-11.22
p_{11}	146.8	174.6	114.2

Table 5.1 shows the calculated values of p_{xx} for plane waves and antenna simulations of the flat samples, as well as p_{xx} for plane waves simulations of the patterned samples.

When comparing the p_{xx} of plane wave and antenna simulation of flat samples, there appears to be a large difference between the two. A comparison of the permittivity models showed that the difference was the highest for a high density thick sample with a peak difference of 4% for the permittivity. This shows that the plane wave assumption is still valid for densities close to the targeted density, but invalid for higher densities. When comparing the p_{xx} values for pattern and flat samples, there is a large difference as expected.

5.3 Measurements

This section will describe the results of the measurements and the construction of the density models. The THz imaging system was used to measure the phase difference with and without sample and the thickness was measured using a slide ruler with micrometer precision. The density of the samples was measured in a previous work by Nabil Souihi [5]. The measurements were inserted into the antenna permittivity model and patterned sample permittivity model in order to obtain the permittivity of the different samples.

5.3.1 Flat Sample

The measured phase difference and thickness of the different flat samples can be seen in table 5.2. Figure 5.8 plots the the known density of the samples versus the calculated permittivity using the antenna permittivity model and the change of phase measured with the THz imaging system. According to section 2.2 there should be a linear relation between density and permittivity, this is confirmed in figure 5.8. The green line that indicates the relation between density and permittivity is:

$$\epsilon' = 1.7926\rho + 0.6120 \tag{5.1}$$

So:

$$\rho = 0.5578\epsilon' - 0.3414 \tag{5.2}$$

Table 5.2: Table shows measurement results for the different Flat Ribbons. Density values taken from [5]

Ribbon	Thickness[mm]	$\Delta\Phi$[degrees]	density[g/cm^3]
N1	1.487	343.9	0.955
N3	0.838	230.6	1.113
N4	1.725	431.0	0.984
N5	1.989	516.3	1.046
N6	0.722	184.3	1.033
N7	2.005	530.5	1.033
N8	1.488	341.9	0.950
N9	0.844	228.8	1.083
N10	1.229	306.1	1.036
N11	1.582	439.2	1.096

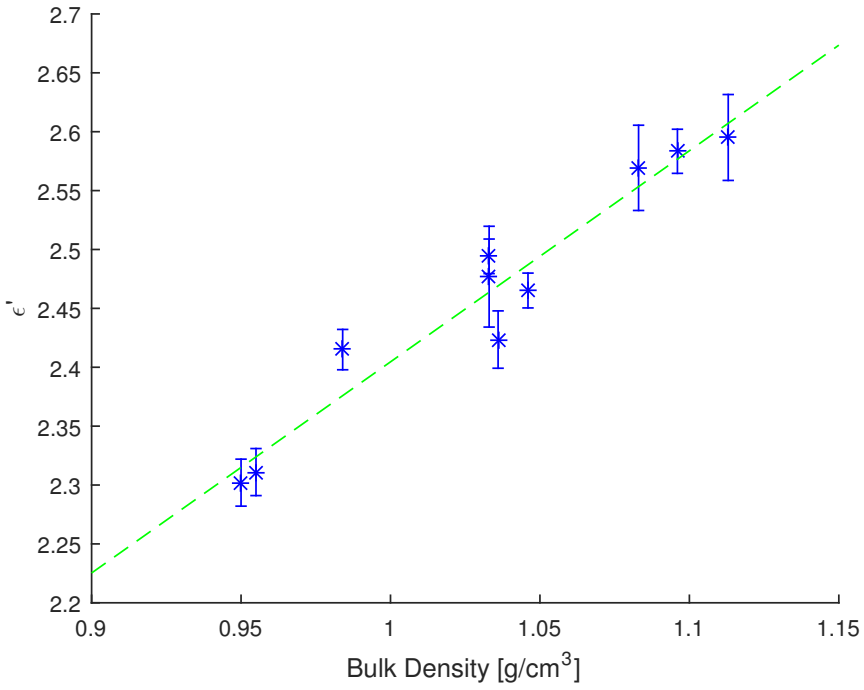

Figure 5.8: The plot shows the known density versus the calculated permittivity using the antenna permittivity model and the experimentally obtained values for the change in phase. The green line depicts the linear regression model of the density-permittivity relation. The errorbars were calculated using the $\pm 5°$ measurement uncertainty seen in figure 3.6b on the measurements. The difference between the errorbars are due to the difference in thicknesses between the samples.

Table 5.3: Table shows measurement results for the different patterned samples. Density values from [5].

Ribbon	Thickness[mm]	$\Delta\Phi$[degrees]	density[g/cm^3]
N4	2.304	500.2	0.984
N7	2.376	540.4	1.033
N10	1.700	355.2	1.036
N11	2.063	490.2	1.096

Using Eq. 2.3 the values for a_f and k can be extracted assuming that ϵ'' is constant at 0.1. Values of $a_f = 0.1634$ and $k = 1.7926$ were obtained.

Using Eq. 2.2 the imaginary part of the permittivity seems to be close to 0.03. However, simulations have confirmed a negligible change in phase difference with the change in permittivity. Making the value of the imaginary part of the permittivity independent of the density so the value does not affect our model.

5.3.2 Patterned Sample

The measured phase difference and thickness of the different pattern samples can be seen in table 5.3. Figure 5.9 depicts the known density of the samples versus the calculated permittivity using the patterned sample permittivity model. Using the same linear regression as in the case of the flat sample, the constructed density model becomes:

$$\rho = 0.6180\epsilon' - 0.4914 \tag{5.3}$$

Note the similarity between the two models of the relation between permittivity and density in Eq. 5.2 & 5.3. This is an expected result since all the samples considered in this study are from the same compound.

5.4 Error Analysis

This section will describe possible error contributions and how they affect the models.

5.4.1 Possible Error Contribution

A number of factors could be contributing to errors in the measurements. As stated in section 3.2, the uncertainty of the phase measurement is $\pm 5°$.

The density may not be constant over the sample. Some of the measured samples exhibited an increasing phase in one direction over the measurement area as seen in figure 5.3. Variations in thickness may also cause the same effect. Table 5.4 shows how the calculated permittivity varies over two different flat samples. While sample 1 is stable and variation can be assumed to be due to the uncertainty of the measurements. Sample 2 however varies significantly over the ribbon. Confirming the fact that density variation occurs across the ribbon.

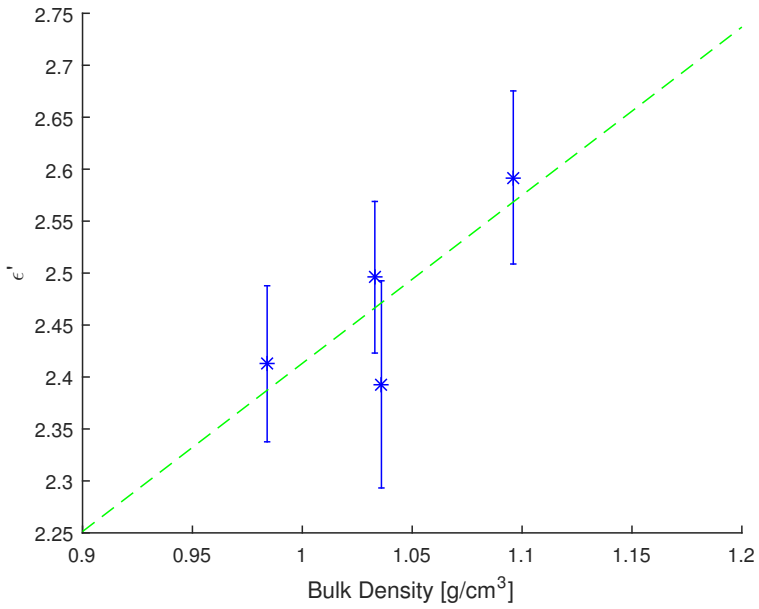

Figure 5.9: The plot shows the known density versus the calculated permittivity using the antenna permittivity model. The green line depicts the linear regression model of the density-permittivity relation. The Error bars indicates the upper and lower limits of the shift in ϵ' when taking the potential errors of $\pm 21°$ into account, see table 5.5.

Table 5.4: Table shows the calculated permittivity using antenna permittivity model for flat ribbons when measuring the left, right and center part of the ribbon.

Part of the ribbon	ϵ' Sample 1	ϵ' Sample 2
Left	2.6748	2.4198
Center	2.6686	2.3693
Right	2.7179	2.5030

Table 5.5: Table shows the uncertainty in degrees with each measurement of a patterned sample. The impact of a deformed pattern will be dependent on the density of the sample.

Error source	[degrees]
Translation [mm]	±8
Rotation [°]	±8
Measurement uncertainty	±5
Deformed pattern	-20

Measuring the thickness of the samples was carried out using a slide ruler with micrometer precision. The ruler is unable to detect thickness variations over an area smaller than the contact area, which was ≈ 0.2 cm^2.

The error contributions to the measurement of the patterned sample include the same factors as the flat samples, but also include specific contributions due to the pattern. The measurement system is sensitive to how the patterned sample is placed in the holder. Small translations along an axis, undetectable by eye, may cause a change of phase up to 8°. Rotation has an estimated impact of 8° for rotations under 10°, since the aim is to place the sample at the same rotation for each measurement, any larger rotation would have been visibly detected. Making the estimated error 21° for patterned samples. A deformed pattern, i.e. changes in the radius of the pattern cylinders will render the measurements invalid.

5.4.2 Model Accuracy

Figure 5.10 displays the error in the density model for the different samples if the maximum estimated error in section 5.4.1 occurs for different thicknesses. Note that the bulk density error decreases with thickness. This is an expected result since the phase difference is larger for thicker samples, thus reducing the impact of the fixed phase error. Also note that the estimated maximum error is ≈ 5 times smaller for flat samples than patterned samples. Since the maximum estimated error for patterned samples is 4 times larger than the flat samples this is expected.

When analyzing the deviation between the density obtained from the density model and the density measured in [5], there is a mean difference of 0.0118 g/cm^3 for flat samples and 0.0243 g/cm^3 for patterned samples. In Table 5.6 we see that the largest deviation is obtained from the measurement of N10 in both models, with a difference of 0.0254 g/cm^3 and 0.0485 g/cm^3 for flat and patterned sample respectively.

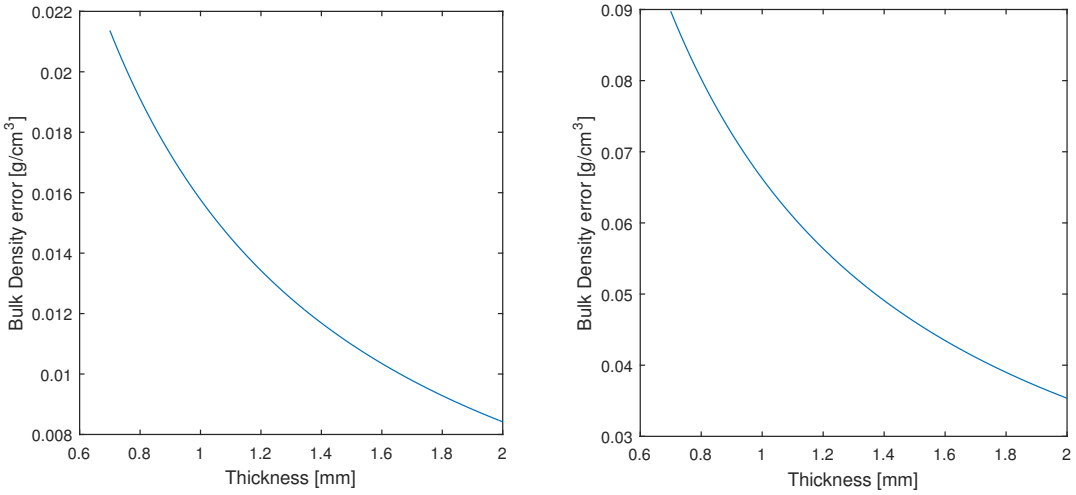

(a) Flat sample **(b)** Patterned sample

Figure 5.10: The figure to the left shows the density error of flat samples for different thicknesses if a measurement error of $\pm 5°$ occurs. The figure to the right shows the density error of patterned samples for different thicknesses if a measurement error of $\pm 21°$ occurs.

Table 5.6: Table shows a comparison between the density model of this thesis and the measured density values using the existing measuring system, taken from [5]. The relative density is the ratio between the density model and the density using the existing setup. (F) and (P) stands for Flat and Patterned sample.

Ribbon Flat/Patterned	Density model [g/cm^3]	density (Existing Setup) [g/cm^3]	Relative ρ
N1(F)	0.9478	0.955	0.9925
N3(F)	1.1063	1.113	0.9940
N4(F)	1.0058	0.984	1.0222
N5(F)	1.0338	1.046	0.9883
N6(F)	1.0404	1.033	1.0071
N7(F)	1.0500	1.033	1.0164
N8(F)	0.9428	0.950	0.9924
N9(F)	1.0919	1.083	1.0082
N10(F)	1.0106	1.036	0.9754
N11(F)	1.0997	1.096	1.0034
N4(P)	0.9997	0.984	1.0160
N7(P)	1.0512	1.033	1.0176
N10(P)	0.9875	1.036	0.9532
N11(P)	1.1106	1.096	1.0133

6
Conclusion

This thesis demonstrates that by using a THz-imaging system it is possible to obtain the density of flat samples over an area of 4 by 4 mm with sufficient precision if the thickness is known. While the system is able to measure patterned sample as well, the alignment sensitivity makes the possible error significant. Since there is a possibility of the patterned sample splitting in the roller compactor, causing the pattern to be removed, the measuring system used in this thesis is not suitable to measure patterned ribbons on-line in its current form..

The ability to measure the average density over and area of 4 by 4 mm is a big improvement from the existing system that measures the average density over an area of 5-8 cm^2. Making possible to observe density variations across the ribbon with higher accuracy. The speed of one measurement has also been increased by a factor of 2.

Though this thesis has shown the ability to obtain the density of a compressed paracetamol formulation, a larger sample size is needed for statistical certainty of the density model, especially in the case of the patterned samples.

6.1 Future work

While the system has shown the possibility of measuring density of the flat samples, there are some ways in which it could be improved. One of the things to consider is to find a way to get rid of the phase ambiguity of the measurements. The phase ambiguity can be removed by using several nearby measuring frequencies [17] and comparing the phase shift between frequencies. This would make possible to measure on thicker samples since the phase ambiguity makes impossible to differentiate between changes in phase larger than $\pm 360°$. Further improvements may include finding a way to measure the thickness of the samples from the measurement setup. This can also be accomplished by measuring multiple frequencies. Without this, there will be no way of placing the setup on-line.

A larger sample size need to be taken to increase the accuracy of the relation between permittivity and density, especially in the case of the patterned samples.

The focus of the thesis was on developing the density measurements. A significant improvement to the system would be to add the moisture content measurement, which needs further simulations and models. A recent work by Vessen Vassilev has shown the possibility of measuring moisture content of thin papper [18].

It would also be of interest to study the density distribution in further detail using a larger sample size and investigating the density across the ribbon over time.

If the cause of the phase drift in the system can be found and improved, it is possible to further reduce the measurement time by a factor of two. One of the candidates is the temperature variation due to the air conditioning turning on and off. Another candidate for high phase drift is the divider circuitry where the logical triggering level might drift with temperature and therefore trigger at different points of the sinusoidal input [6].

Bibliography

[1] Asncombe, N. *No place to hide [millimeter wave imaging]*, IEE Review VOL. 51 , NO 12, December 2005

[2] Peter H. Siegel *THz Instruments for Space*, IEEE Transactions on Antennas and Propagation, VOL. 55, NO. 11, November 2007

[3] Calvin Yu et al. *The potential of terahertz imaging for cancer diagnosis: A review of investigations to date* Quantative Imaging in Medicine and Surgery, Vol. 2, NO. 1, March 2012

[4] Robert K. May et al. *Hardness and Density Distributions of Pharmaceutical Tablets Measured by Terahertz Pulsed Imaging* Journal of Pharmaceutical Sciences, VOL. 102, NO. 7, July 2013

[5] Nabil Souihi et al. *Roll compaction process modeling: Transfer between equipment and impact of process parameters* International Journal of Pharmaceutics, Vol. 484, no 1-2, February 2015

[6] Robin Dahlbäck *Sub-millimetre wave imaging*. Master Thesis, Chalmers University of Technology, 2011

[7] Hiltmar Schubert and A. Rimski-Korsakov et al. *Stand-off Detection of Suicide Bombers and Mobile Subjects* The NATO programme for Security through Science, Springer Science Business Media, 2006

[8] Roger Appleby et al. *Standoff detection of weapons and contraband in the 100 GHz to 1 THz region* IEEE Transactions on Antennas and Propagation, vol. 55, no. 11, 2007.

[9] Sophocles J. Orfanidis *Electromagnetic Waves and Antennas*, Rutgers University, 1999

[10] David M. Pozar *Microwave Engineering*, 4th ed. Amherst: John Wiley & Sons, Inc., 2012

[11] Samir Trabelsi et al. *Online Determination of Bulk Density and Moisture Content* IEEE Transactions on Instrumentation and Measurement, VOL. 47, NO. 1, February 1998

[12] Samir Trabelsi et al. *Microwave Sensing Method for Simultaneous and Independent Determination of Bulk density and Moisture content of Shelled Peanuts*, IEEE Antennas and Propagation Society International Symposium July 2006

[13] Stuart O. Nelson et al. *Measurement of Grain and Seed Moisture and Density Through Permittivity Relationships* IEEE Instrumentation and Measurement Technology Conference (I2MTC) 2010

[14] Samir Trabelsi et al. *Microwave dielectric sensing of bulk density of granular materials* Measurement Science and Technology, Vol. 12, November 2001

[15] Samir Trabelsi et al. *New Density-Independent Calibration Function for Microwave Sensing of Moisture Content in Particulate Materials* IEEE Transactions on Instrumentation and Measurement VOL. 47, NO 3, 1998

[16] Robin Dahlbäck *A System for THz Imaging of Low-Contrast Targets Using the Born Approximation*. IEEE Transactions on Terahertz Science and Technology, VOL. 2, NO. 3, May 2012

[17] Samir Trabelsi et al. *Phase-Shift Ambiguity in Microwave Dielectric Properties Measurements* IEEE Transactions on Instrumentation and Measurement, VOL. 49, NO. 1, February 2000

[18] Vessen Vassilev et al *A mm-Wave Sensor for Remote Measurement of Moisture in Thin Paper Layers* IEEE Transactions on Terahertz Science and Technology, VOL. 5, NO. 5, Sep 2015